Hindawi
Laser and Particle Beams
Volume 2022, Article ID 2455226, 9 pages
https://doi.org/10.1155/2022/2455226

*Research Article*

# Numerical Simulation and Validation of Multiscale 3D Laser Spiral Machining of Microholes

**Yiwei Dong**,[1] **Qianwen Ye**,[1] **Qi Li**,[2] **Xiang Guo**,[1] **Saitao Zhang**,[1] **and Naixian Hou**[3]

[1]*School of Aerospace, Xiamen University, Xiamen 361005, Fujian Province, China*
[2]*ENN Energy Power Technology (Shanghai) Co., Ltd, Shanghai 201306, China*
[3]*AECC Commercial Aircraft Engine Co., Ltd, Shanghai 200241, China*

Correspondence should be addressed to Yiwei Dong; ywdong@mit.edu

Received 25 October 2021; Revised 1 January 2022; Accepted 18 January 2022; Published 9 March 2022

Academic Editor: Dimitri Batani



Femtosecond laser ablation is widely applied in high-precision machining of microholes in aeroengine turbine blades. To further explore the mechanism of action during the laser processing of microholes, numerical simulations were performed on the basis of a molecular dynamics (MD) method coupled with a two-temperature model (TTM). Laser irradiation on the surface of copper for different femtosecond-laser processing parameters is investigated in this work. Through the femtosecond-laser single-pulse central ablation simulation model, the laser energy flux density in a Gaussian laser spot range was discretized and analyzed to calculate the ablation depth at multiple points separately. The cross-sectional morphology of the femtosecond-laser single-pulse ablation pits was approximated and fitted. Finally, a 3D simulation model of the whole process of multiscale femtosecond-laser spiral processing microholes was established by superimposing multipulse femtosecond-laser spiral trajectories. This provides a theoretical basis for analyzing the evolution of geometric parameters and morphological characteristics of the hole during machining with specific laser and process parameters.

## 1. Introduction

The machining accuracy and quality of microholes are crucial for improving microhole efficiency and guaranteeing engine energy efficiency. However, the existence of microholes damages the structural integrity of turbine blades. The stress concentration around the hole and the microstructural defects of the hole wall caused by the hole-making process cause film-cooling holes to be the most frequent cause of blade failure [1]. Hence, an effective technology for microhole processing is of great significance [2].

In recent years, Laser drilling is widely used in many neighborhoods as a controllable machining technology based on laser ablation [3]. Especially femtosecond laser processing has become one of the mainstream technologies for turbine-blade microhole processing due to its various advantages, such as being ultrafast and ultraintense as well as having a small heat-affected zone [4]. Based on numerical simulations of the femtosecond laser ablation of metal targets, researchers have conducted many theoretical studies on the energy transfer within the material and the subsequent ablation process of the material [5–10]. To better elaborate on the physical nature of the femtosecond laser ablation of metallic materials, some researchers have proposed a two-temperature model with molecular dynamics (TTM-MD) [11–13]. It can characterize both the absorption of the laser energy by electrons inside the material and the energy exchange processes between electrons and lattice systems after ultrafast laser irradiation of the surfaces of metallic materials. Furthermore, it describes the material phase transition processes at the atomic/molecular level after lattice thermalization. Dong et al. [14] investigated the ablation depth of the focal point moving downward at different velocities at different pulse intervals by means of a modified two-temperature equation. Li et al. [15] introduced a 3D two-temperature model (TTM) to simulate femtosecond ablation on the aluminum film to investigate the three-dimensional temperature evolution of electrons lattices and precisely predict the shape hole before ablation take place. Foumani et al. [16] used TTM-MD to investigate the responses of copper films at different laser energy densities. Based on the simulations using this model, the dependence of the copper film reflectivity on the laser energy flux and the evolution of the thickness, electron temperature, and lattice temperature with time were calculated. Previous studies often focused on the ablation mechanism of single or multiple pulses to explore the evolution of small holes forming. These studies were limited to the research scale and by other factors. The development of theoretical models is still immature, and the existing models are difficult to use to guide engineering practice.

In the process of femtosecond laser hole drilling, in addition to the influence of the material properties and the process parameters during laser ablation, the process also has a significant impact on the processing quality [17–20]. Research around the world on the femtosecond laser hole-making process mainly focuses on two aspects: annular cutting and spiral processing [21]. See et al. [22] at the University of Manchester established a preliminary quantitative mapping relationship between the laser energy parameters and the hole diameter and depth based on many physical experiments of femtosecond laser drilling on single-crystal nickel-based alloy specimens. Mishra et al. [23] analyzed the effects of the geometric parameters, such as hole depth and taper, on the propagation characteristics of subsequent pulses. They established a two-dimensional axisymmetric finite element model for multipulse laser perforations. The optimal combination of laser parameters based on experimental data was confirmed using a neural network and gray correlation analysis, which enabled the effective control of the taper of small holes and the extent of the heat-affected zone. A research team from Huazhong University of Science and Technology investigated the effect of relative motion between a laser and material on hole formation. At the University of Stuttgart, Germany, physical experiments on annular drilling were conducted based on a four-light wedge rotation system, demonstrating that the quality achieved by annular drilling was significantly improved compared to that by percussion drilling [24]. Yin et al. [25] found that femtosecond laser spiral machining can better handle high depth-to-diameter ratio holes, but the relationship between the geometric evolution process of small hole formation and the main processing parameters during spiral hole making is unclear. Moreover, there is a lack of model guidance for the optimization of processing parameters.

Based on the TTM-MD model, the ablation process of the surface of copper material irradiated by a femtosecond laser is simulated in this paper. The influence of different laser energy parameters on the ablation mechanism of the material is revealed, and the ablation depth is calculated. In addition, according to the mapping relationship between the femtosecond laser energy parameters and the ablation morphology, combined with the analysis of the laser focus trajectory during processing, a multiscale three-dimensional (3D) model of the whole process of femtosecond laser spiral processing of microholes is established. The study provides model support and a theoretical basis for the process optimization of the femtosecond laser spiral processing of microholes.

## 2. Calculation Model

*2.1. Combined Two-Temperature Model with Molecular Dynamics (TTM-MD).* The TTM-MD model is widely used to describe the mechanism of action of femtosecond laser irradiation on the surfaces of metallic materials [26]. The conventional TTM describes the evolution of the energy between photons, electrons, and lattices by two coupled nonlinear differential equations. Electrons are excited by the laser, and the ion-lattice system is then heated through electron collisions which transfer their energy [27]. Molecular dynamics (MD) describes the phase transitions that occur during metal ablation and the material removal process at the atomic scale. MD compensates well for the shortcomings of the TTM in the description of phase transitions. Thus, a combination of the two is considered. The equations of the TTM-MD are as follows:

$$\begin{aligned} C_e\frac{\partial T_e}{\partial t} &= \frac{\partial}{\partial x}\left(k_e\frac{\partial T_e}{\partial x}\right) - G\left(T_e - T_l\right) + S(x,t), \\ m_i\ddot{r}_i &= F_i + \xi m_i V_i^T, \end{aligned} \tag{1}$$

where $C_e$ and $C_l$ represent the electron and lattice heat capacities, respectively, $T_l$ and $T_e$ represent the lattice and electron temperatures, respectively. Thus, $k_e$ is the thermal conductivity which varies with the ratio of electron temperature over lattice temperature, and $G$ is the electron-phonon coupling coefficient. $S(x, t)$ is the laser source term, which represents the laser energy input. It is represented as follows:

$$S(x,t) = \frac{A\alpha F}{\sqrt{\pi/4\ \ln(2)}t_p}\cdot\Theta, \tag{2}$$

where

$$\Theta = e^{-\alpha x}e^{-4\ln(2)\left(t/t_p - 2\right)^2}, \tag{3}$$

where $A$ is the surface transmittance, $t_p$ is the pulse width, $\alpha$ is the absorption coefficient of the material, $F$ is the energy flux of the laser, and $x$ is the distance of the calculated position from the surface position of the material. $m_i$ and $r_i$ represent the mass and displacement of the first atom, respectively, $F_i$ is the force exerted between atoms, $\dot{r}_i$ is the first-order derivative of the displacement with respect to time, $\ddot{r}_i$ is the second-order derivative of the displacement with respect to time, and $\xi$ is the velocity equilibrium factor. $\xi$ is expressed as follows [11]:

$$\xi = \frac{1}{n}\frac{\sum_{k=1}^{n} GV_N\left(T_e^k - T_l\right)}{-\sum_i m_i\left(V_i^T\right)^2}, \tag{4}$$

where $n$ is the number of atoms, $V_N$ is the volume of each layer of atoms, and $V_i^T$ is the speed of thermal motion of the atoms.

https://doi.org/10.1155/2022/2455226 Published online by Cambridge University Press

*2.2. Atomic-Level Simulation System.* Metallic copper is widely used in modern industry, and its thermal physical parameters are relatively well known. Thus, metallic copper was selected as the simulation object in the model for theoretical study to establish the atomic level system. Copper crystals are face-centered cubic (fcc), and the typical atomic distribution of this fcc stacking structure is shown in Figure 1.

In the investigation of the effect of changing the single-pulse laser parameters on the changes of the temperature field and the ablation results of the system, the model size was 6a × 6a × 150a, corresponding to actual sizes of 2.619 nm × 2.619 nm × 54.225 nm, and the total atomic number of the system was 21,600. In the calculation of the ablation depth, it is necessary to increase the size of the system. The model size was expanded to 6a × 6a × 500a, corresponding to an actual size of 2.619 nm × 2.619 nm × 180.75 nm, and the total atomic number of the system was expanded to 72,000.

Due to the enormous spatial scale spanning from the atomic level to the macroscopic level, the computational volume of the MD simulation would increase dramatically with the increase in the system size. Limited by the computational volume, the size range of an MD simulation system is much smaller than an actual laser irradiation area. Therefore, periodic boundary conditions (PBC) were used around the simulation region, which were infinitely expandable in all directions, thus significantly reducing the computational effort while ensuring computational accuracy. Under the PBCs, atoms leaving from one side of the boundaries at a certain speed will enter from the opposite side of the boundary at the same rate, thus ensuring a constant number of atoms in the whole system and effectively eliminating the effect of the boundary effects.

Laser energy has a spatial distribution along the laser propagation direction [28]. When exploring the effect of changing the parameters of the single-pulse laser on the temperature field change and ablation results of the system, free boundary conditions were used at both ends of the simulated region, and the atoms were free to move in this direction to facilitate the study of the material evolution process at the atomic level, which corresponded to the actual irradiation and ablation process of a metal film by a femtosecond laser.

When calculating the ablation depth, free boundary conditions were used at the top of the laser incidence, fixed boundary conditions were used at the bottom, and a constant-temperature heat bath at 300 K was added. The laser energy transmitted to the bottom was absorbed, and the energy was considered to be transferred deeper into the material, thus more accurately simulating the ablation of the block target by the femtosecond laser. The dimensions and boundary conditions of the models are shown in Figure 2.

A system with a fixed atomic number but not a fixed energy is considered, and the canonical ensemble was chosen for the MD simulations. In addition, in the MD simulations, different potential functions should be used for different substances. Due to the special nature of metallic materials, the two-body or three-body potential between

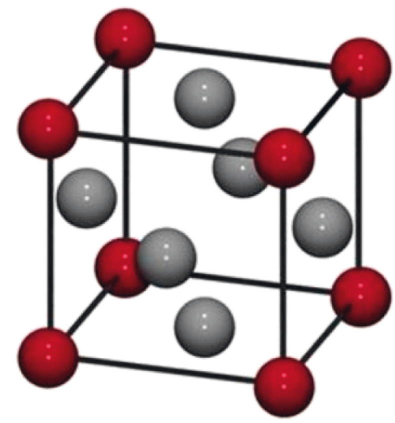

Figure 1: Schematic diagram of a single cell of a copper crystal.

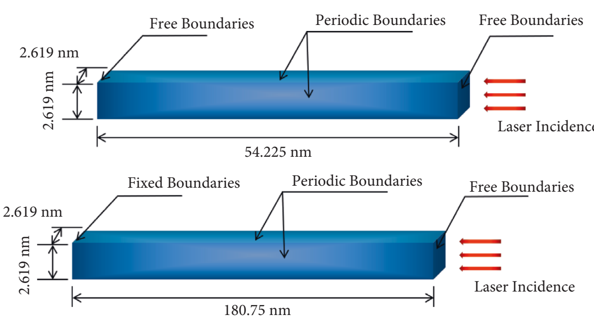


Figure 2: Dimensions and boundary conditions of the model.

atoms cannot accurately describe the interparticle forces within the metal and thus cannot achieve the computational accuracy required. The potential function that is commonly used is embedded atom model (EAM) [6, 29]. According to the density functional theory (DFT), the nucleus will be affected by the electrostatic effect of the background electron cloud in addition to the repulsion of other nuclei in the system. Therefore, the potential function can be divided into two parts: the interaction energy between the nuclei and the mosaic energy of the nuclei with the background electron cloud. The first part can be approximated by a two-body potential, while the second part is a multibody interaction and cannot be approximated by a two-body potential. The mathematical expression for the embedded atomic potential is as follows:

$$V_i = \frac{1}{2}\sum_{i\neq j}\phi_{\alpha\beta}\left(r_{ij}\right) + F_\alpha\left(\sum_{i\neq j}\rho_\alpha\left(r_{ij}\right)\right), \tag{5}$$

where $F_\alpha$ is the embedding function, which is the energy required to embed an atom $i$ of type $\alpha$ in the electron cloud, $\rho_\alpha$ is the electron density generated at the $\alpha$-type atom, $r_i j$ is the distance between the two atoms, and $\phi_{\alpha\beta}$ is the two-body potential between the $\alpha$-type and $\beta$-type atoms.

## 3. Results and Discussion

*3.1. Effect of Different Process Parameters on Ablation Mechanism.* The laser parameters are listed in Table 1.

https://doi.org/10.1155/2022/2455226 Published online by Cambridge University Press

Table 1: Different energy densities for femtosecond laser ablation.

| Group | Pulse width (fs) | Energy flux ($J/m^2$) |
|---|---|---|
| 1.1 | 300 | 1000 |
| 1.2 | 300 | 2232 |
| 1.3 | 300 | 3188 |
| 1.4 | 300 | 4782 |

Figure 3 shows the electron temperature curves and lattice temperature curves of the material surface under different laser energy flux conditions. Due to the fixed laser pulse width, the maximum temperature of the lattice increased with the increase in the pulse energy. The electron temperature all reached the highest temperature at 0.3 ps, and the maximum temperature of the lattices all appeared at 1.4 ps.

The atomic snapshots after VMD visualization and stitching are illustrated in Figure 4. The film did not undergo a phase transition after laser energy injection, but a slight periodic elongation and shortening phenomenon occurred. This phenomenon was explained by the fact that, at lower energy densities (1000 $J/m^2m^2$), the lattice temperature at which the electron-lattice system was in equilibrium was low and was not sufficient to cause the material to undergo a phase transition. When the laser energy flux increased to 2232 $J/m^2$, as shown in Figure 4(b), the surface on that side of the laser irradiation showed partial ablation, and a certain number of atoms were removed from the surface of the film (circle 1 in Figure 4(b)), followed by a more pronounced thermal expansion effect of the film. Figure 4(c) shows that when the laser energy flux increased to 3188 $J/m^2m^2$, the ablation was more intense, clusters of atoms were removed from the system (circle 1 in Figure 4(c)), and primary nucleation within the material was evident (circle 2 in Figure 4(c)). As shown in Figure 4(d), when the laser energy flux was further increased to 4782 $J/m^2$, the film first underwent intense thermal expansion at 0–5 ps. Furthermore, a large number of atoms broke away from the system, with more nucleation and more intense melting inside the material. The solid mechanical stress caused by the thermal expansion and the melting inside the material caused the film to undergo lamellar cracking.

*3.2. Effect of Different Process Parameters on Ablation Mechanism.* To better understand the ablation process and to relate the numerical simulation results to the actual punching process, it is necessary to calculate the ablation depth. Increasing the calculation system and the calculation time step is essential to obtain more effective simulation results. In the calculation of the ablation depth, the laser parameters were set, as shown in Table 2.

The ablation depths of copper under irradiation with single-pulse femtosecond laser irradiation at different energy densities are shown in Figure 5.

Figure 5(a) shows the atomic snapshot of the expanded system within 120 ps after irradiation by a single pulse with an energy flux 3188 $J/m^2$. The system expanded rapidly within 0–10 ps and generated bubbles by an internal phase transformation. A large number of atoms broke away from the system. The maximum depth of the bubble nucleation was about 20 nm from the surface, and the bubbles continued expanding until the material underwent layer cracking. With an increase in the energy flux to 4782 $J/m^2$, at 10 ps, many atomic clusters already appeared at the melting front of the laser incident surface, and a violent phase transition occurred inside the material. The maximum nucleation depth was about 25 nm, and the layer cracking effect was more evident at the laser energy density of 3188 $J/m^2$. The etching of the material was complete at 40 ps, and the thermal expansion of the material continued. After 100 ps, the effect of the laser on the material stopped. The ablation depth of the material was 16 nm, as illustrated in Figure 5(b). As shown in Figure 5(c), with the increase in the laser energy flux to 6377 $J/m^2$, the phase change on the material surface was more intense. Furthermore, due to the further growth of the lattice superheat ratio, the lattice disorder on the material surface was more significant. The cavities were denser, with more clusters of atoms leaving the system at 10 ps, and the farthest bubble was generated 32 nm from the surface. The material underwent more lamellar cleavage during the etching process, and the thermal expansion effect disappeared at 100 ps. However, some atoms continued leaving the system, and the ablation depth was 22 nm at this time. The ablation depth and intensity of the material both increased with the laser energy flux. To investigate the relationship between the ablation depth of the material and the laser energy flux, the laser energy flux continued to increase to 7971 $J/m^2$. A new atomic snapshot was formed, as shown in Figure 5(d). Within 10 ps, the lattice 20 nm from the surface rapidly began to become disordered, more material was etched away, and the final ablation depth reached 47 nm.

The variations of the ablation depth with the laser energy flux in the simulated ablation results and physical ablation experiments from the literature are compared in Figure 6 [30]. The calculated values of the laser ablation depth in the laser energy range simulated in this paper were in excellent agreement with the experimental values from the literature, further verifying the model's accuracy. The ablation depths induced by a single pulse of the femtosecond laser were all on the nanometer scale. There are often thousands of vibrations in actual gas-film-hole femtosecond laser spiral processing, so more factors need to be taken into account. A complete multiscale simulation model of the microhole femtosecond laser spiral processing will be developed as follows.

*3.3. Simulation Model of Whole Process of Multiscale Three-Dimensional (3D) Laser Spiral Machining of Air Film Holes.* Limited by the scale of the computational space, the above MD simulations only showed the ablation depth of the material at the center of the spot during the single-pulse ablation of the femtosecond laser. The size was only on the order of tens of nanometers, while the sizes of spots and complete ablation pits are typically on the order of microns. This scale gap makes it almost impossible to directly predict the ablation crater morphology of femtosecond-laser single-

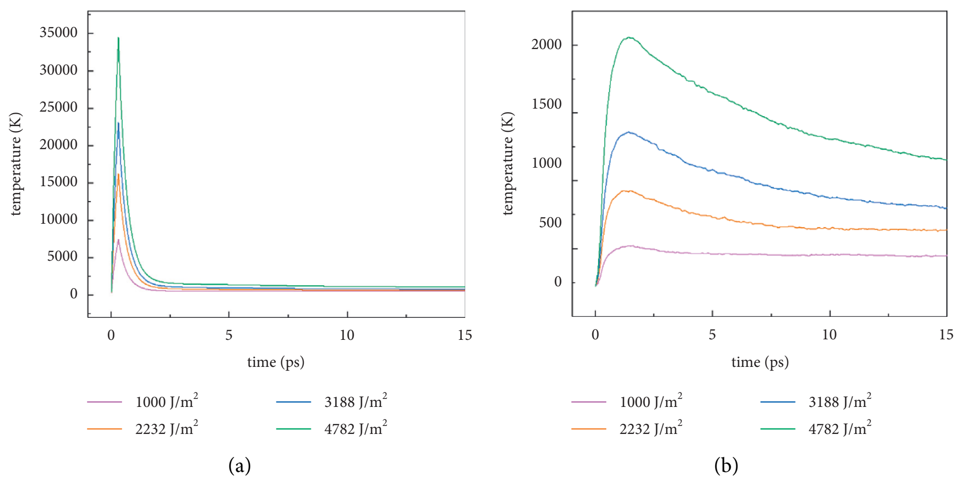


FIGURE 3: Surface electron and lattice temperatures at different energies: (a) surface electron temperature and (b) surface lattice temperature.

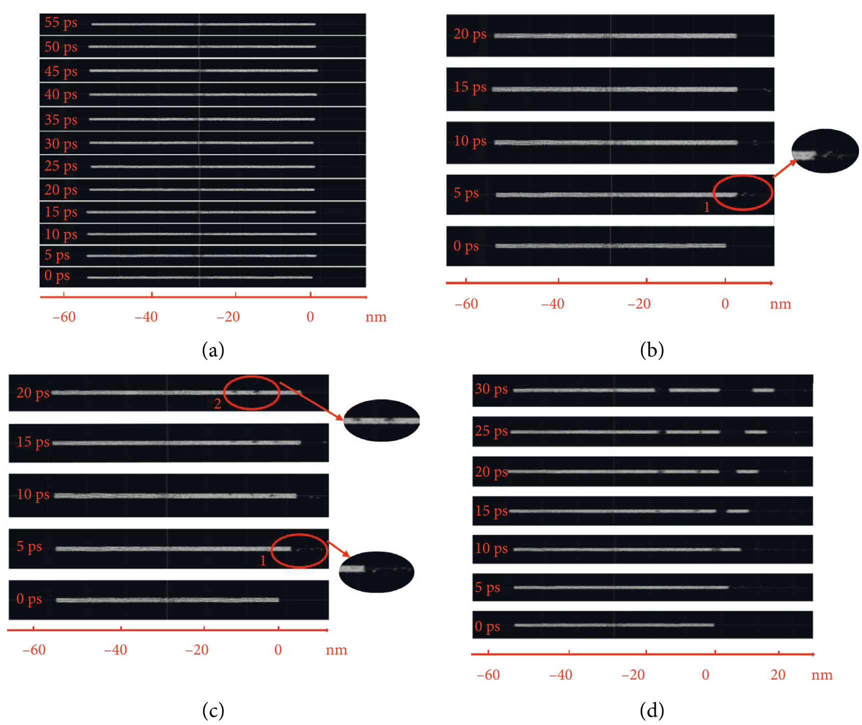


FIGURE 4: Schematic diagram of atomic snapshots at different energy flux: (a) 1000 J/m$^2$, (b) 2232 J/m$^2$, (c) 3188 J/m$^2$, and (d) 4782 J/m$^2$.

TABLE 2: Laser parameter settings for the second group of calculations.

| Group | Pulse width (fs) | Energy flux (J/m$^2$) |
|---|---|---|
| 2.1 | 300 | 3188 |
| 2.2 | 300 | 4782 |
| 2.3 | 300 | 6377 |
| 2.4 | 300 | 7971 |

pulse ablation by MD simulations. An approximate simulation method for predicting the ablation crater morphology of Gaussian-type femtosecond laser pulses—the 'patchwork method'—was proposed [31]. The methods assumed that the energy distribution of the laser spot obeys a Gaussian distribution, and different distances from the center of the spot will correspond to different laser energy flux. This can produce different ablation depths, and the calculated results from different locations are spliced to obtain the approximate ablation pit morphology. Different from this, this paper improves the patchwork method by using polynomial fitting to fit polynomial curves to multiple discrete "laser energy density-ablation depth" calculations to obtain a complete morphological characterization of femtosecond laser single-pulse ablation pits. The simulation results of the laser energy flux and ablation depth calculated above are listed in Table 3. It was assumed that 7971 J/m$^2$ was the peak energy flux of the

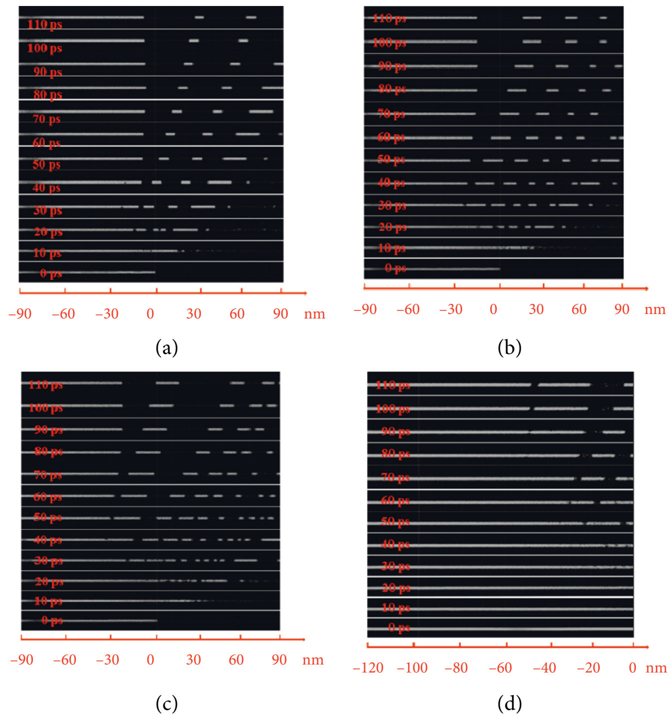


FIGURE 5: Schematic diagram of atomic snapshots at different energy densities: (a) 3188 J/m$^2$, (b) 4782 J/m$^2$, (c) 6377 J/m$^2$, and (d) 7971 J/m$^2$.

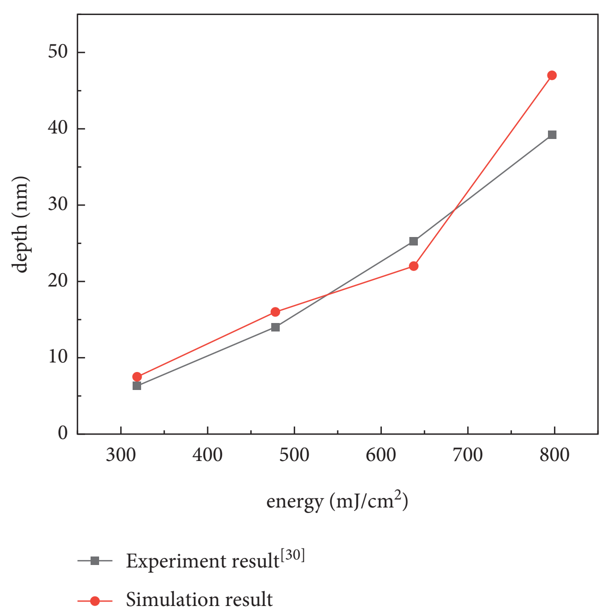


FIGURE 6: Comparison of ablation depth with laser energy.

TABLE 3: Laser energy flux and ablation depth simulation results.

| Energy flux | Ablation depth (nm) |
|---|---|
| 3188 J/cm$^2$ | 7.5 |
| 4782 J/cm$^2$ | 16 |
| 6377 J/cm$^2$ | 22 |
| 7971 J/cm$^2$ | 47 |

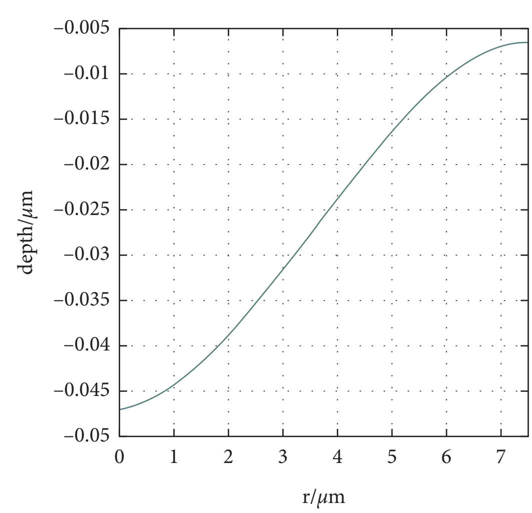


FIGURE 7: Femtosecond-laser single-pulse ablation crater morphology fitting results.

laser, and polynomial curve fitting was performed on several sets of data to obtain complete single-pulse ablation crater morphology of the femtosecond laser, as shown in Figure 7.

The laser beam was scanned along a specific trajectory to achieve layer-by-layer material removal and ultimately achieve particular processing requirements in the laser spiral processing of microholes. For the femtosecond-laser spiral processing of microholes, an optical wedge system is commonly used to control the laser optical path. The laser beam moves along the laser trajectory. Since the laser source is a pulsed laser, the motion of the spot on the irradiated material surface is discontinuous from a microscopic perspective. The spot center is distributed along an Archimedean spiral.

https://doi.org/10.1155/2022/2455226 Published online by Cambridge University Press

Table 4: Femtosecond-laser spiral machining process parameters.

| Parameter | Value |
|---|---|
| Pulse width | 250 fs |
| Repetition frequency | 10 kHz |
| Rotational angular velocity | 3000 rpm |
| Spot diameter | 15 $\mu$m |
| Number of spot trajectory turns | 10 |
| Maximum spot trajectory radius | 100 $\mu$m |

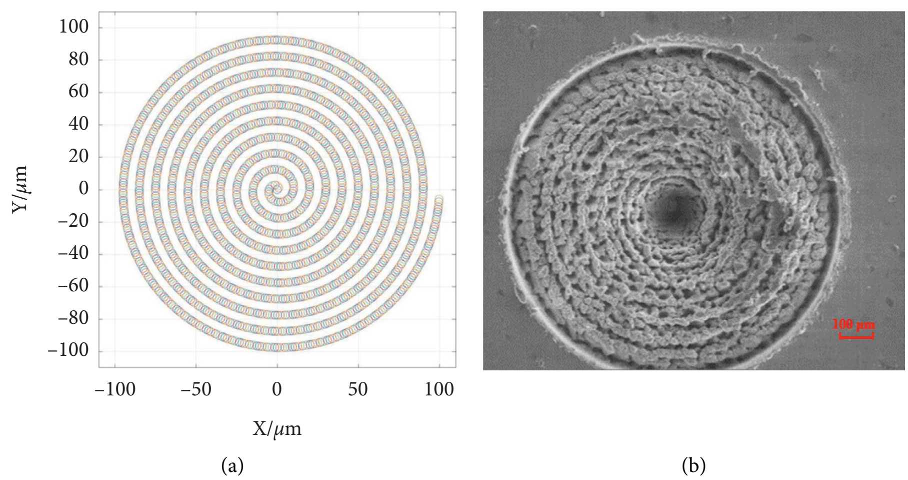


Figure 8: Distribution of spot centers of multiple laser pulses: (a) simulation and (b) actual processing.

Based on the actual system, the equal-linear-velocity case was considered in this paper when modeling the femtosecond-laser spiral processing. The spot center had a uniform moving rate in the plane. The spot centers of multiple laser pulses were distributed equidistantly along an Archimedean spiral. The distances between two adjacent spots were equal, and the overlap rate was kept constant. The actual femtosecond laser spiral processing process parameters are shown in Table 4. Based on the characterization of the laser trajectory of this paper, the distribution of the spot center of multiple laser pulses is plotted in Figure 8(a), and the actual processing of the spot center distribution is shown in Figure 8(b), where each small circle represents a spot. Comparing the two figures, the spot center distribution trend was basically the same.

Based on the results from fitting the morphology of the single-pulse ablation crater of the femtosecond laser and the analysis of the spot distribution in the spiral trajectory of the multipulse femtosecond laser, the simulation calculation of the whole process of spiral processing of the microholes by the femtosecond laser was carried out. Figure 9 shows the simulation results of the central cross section of the microholes obtained by femtosecond-laser spiral processing with the given laser parameters. After one layer of spiral machining, the maximum machining depth of about 500 $\mu$m was obtained near the center. The depths of the holes generally tended to decrease along the radial direction, but there were small fluctuations. The local ablation depth exhibited a slight sudden increase, the ablation depth did not

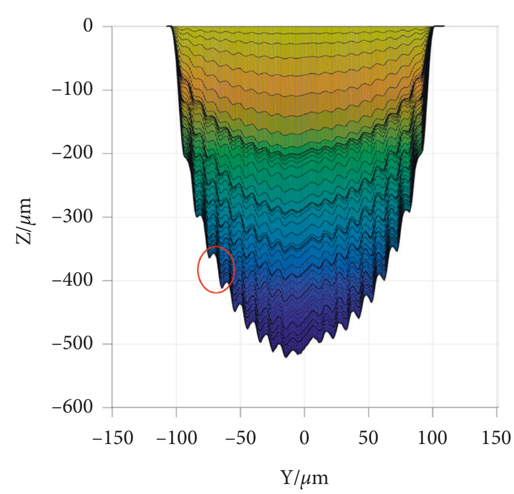


Figure 9: Simulation of the central cross section of the film-cooling hole obtained by femtosecond-laser spiral processing.

strictly decrease along the radial direction, and the entrance diameter of the hole was around 200 $\mu$m. As the spot moved from inside to outside along the spiral track for ablation, the spot density at the center of a hole was significantly higher than that at the edge. The number of ablations at a point near the center was higher than that at points at the border, so the depth of ablation is greater at the center of the hole than at the edge. The sudden increase in the local depth can be attributed to the direct passage of the spot center, resulting in a better local ablation effect than that between the spot

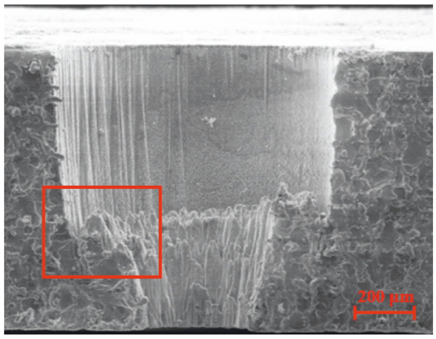


Figure 10: Schematic diagram of the actual ablation cross-section structure.

trajectories. The impact of the spiral trajectory is evident in many locations in the figure (such as the area shown by the circle in Figure 9). The above simulation results qualitatively revealed the direct influence of the femtosecond-laser spiral trajectory on the formation results of microholes. In addition, the actual ablation cross section was shown in Figure 10, where the red box was the abnormal protrusion that occurred during the actual machining process. Comparing the simulated results with the actual ablation results, the trends roughly matched.

## 4. Conclusion

In this paper, the effects of different laser energy flux on the copper ablation process are investigated based on TTM-MD. In addition, a cross-scale 3D simulation model of the whole process of femtosecond laser spiral processing was established. The main conclusions are as follows:

(1) When the laser energy flux is small, the superposition of the tensile stress wave generated inside the material and the unloaded compressive stress wave will cause the copper film to produce periodic stretching; as the laser energy flux increases, more holes will be formed inside the material, the phase transition will become more and more intense, and more atomic clusters will break away from the material surface.

(2) Based on the quantitative mapping of laser parameters-single pulse ablation crater morphology, superimposed on the characterization of femtosecond laser spiral trajectory, a cross-scale simulation model of the whole process of femtosecond laser spiral processing of microsmall holes is established. The model can be used to analyze the geometric parameters and morphological evolution of the hole during processing with specific laser parameters and process parameters.

## Data Availability

The numerical simulation data for laser spiral machining of microholes used to support the findings of this study are included within the article.

## Ethical Approval

This article does not contain any studies with human participants or animals performed by any of the authors. Informed consent was obtained from all individual participants included in the study.

## Conflicts of Interest

The authors declare that they have no conflicts of interest.

## Acknowledgments

This work was financially supported by the National Natural Science Foundation of China (Grant no. 51705440), the Natural Science Foundation of Fujian Province, China (Grant no. 2019J01044), and the National Science and Technology Major Project of China (nos. J2019-III-0008 and J2019-VII-0013-0153).

## References

[1] J. Liu, Z. F. Yue, and Y. S. Liu, "Surface finish of open holes on fatigue life," *Theoretical and Applied Fracture Mechanics*, vol. 47, no. 1, pp. 35–45, 2007.

[2] Z. Zhang, Z. Yang, C. Wang, Q. Zhang, S. Zheng, and W. Xu, "Mechanisms of femtosecond laser ablation of Ni3Al: molecular dynamics study," *Optics & Laser Technology*, vol. 133, Article ID 106505, 2021.

[3] K. Xia, N. Ren, Q. Lin et al., "Experimental investigation of femtosecond laser through-hole drilling of stainless steel with and without transverse magnetic assistance," *Applied Optics*, vol. 60, no. 5, pp. 1399–1410, 2021.

[4] P. Balling and J. Schou, "Femtosecond-laser ablation dynamics of dielectrics: basics and applications for thin films," *Reports on Progress in Physics*, vol. 76, no. 3, Article ID 036502, 2013.

[5] S. Amoruso, "Modeling of UV pulsed-laser ablation of metallic targets," *Applied Physics A: Materials Science & Processing*, vol. 69, no. 3, pp. 323–332, 1999.

[6] P. A. Atanasov, N. N. Nedialkov, S. E. Imamova et al., "Laser ablation of Ni by ultrashort pulses: molecular dynamics simulation," *Applied Surface Science*, vol. 186, no. 1-4, pp. 369–373, 2002.

[7] C.-L. Chang, C.-W. Cheng, and J.-K. Chen, "Femtosecond laser-induced periodic surface structures of copper: experimental and modeling comparison," *Applied Surface Science*, vol. 469, pp. 904–910, 2019.

[8] Y. C. HirayamaI, P. A. Atanasov, M. Obbara, N. N. Nedialkov, and S. E. Imamova, "Femtosecond laser ablation of crystalline iron: experimental investigation and molecular dynamics simulation," *Japanese Journal of Applied Physics*, vol. 459, no. 2R, p. 792, 2006.

[9] N. Maharjan, W. Zhou, Y. Zhou, and Y. C. Guan, "Ablation morphology and ablation threshold of Ti-6Al-4V alloy during femtosecond laser processing," *Applied Physics A*, vol. 124, no. 8, pp. 1–10, 2018.

[10] M. Saghebfar, M. K. Tehrani, S. M. R Darbani, and A. E. Majd, "Femtosecond pulse laser ablation of chromium: experimental results and two-temperature model simulations," *Applied Physics A*, vol. 123, no. 8, pp. 1–9, 2017.

[11] D. S. Ivanov and L. V. Zhigilei, "Combined atomistic-continuum modeling of short-pulse laser melting and

disintegration of metal films," *Physical Review B: Condensed Matter*, vol. 68, no. 6, 2003.

[12] D. S. Ivanov and L. V. Zhigilei, "Combined atomistic-continuum model for simulation of laser interaction with metals: application in the calculation of melting thresholds in Ni targets of varying thickness," *Applied Physics A-Mater,* vol. 79, no. 4-6, pp. 977–981, 2004.

[13] L. V. Zhigilei, Z. Lin, and D. S. Ivanov, "Atomistic modeling of short pulse laser ablation of metals: connections between melting, spallation, and phase explosion," *Journal of Physical Chemistry C*, vol. 113, no. 27, pp. 11892–11906, 2009.

[14] Y. Dong, Z. Wu, Y. You, C. Yin, W. Qu, and X. Li, "Numerical simulation of multi-pulsed femtosecond laser ablation: effect of a moving laser focus," *Optical Materials Express*, vol. 9, no. 11, pp. 4194–4208, 2019.

[15] Q. Li, H. Lao, J. Lin, Y. Chen, and X. Chen, "Study of femtosecond ablation on aluminum film with 3D two-temperature model and experimental verifications," *Applied Physics A*, vol. 105, no. 1, pp. 125–129, 2011.

[16] A. A. Foumani and A. R. Niknam, "Atomistic simulation of femtosecond laser pulse interactions with a copper film: effect of dependency of penetration depth and reflectivity on electron temperature," *Journal of Applied Physics*, vol. 123, no. 4, 2018.

[17] Y. You, Y. Dong, X. Li, Q. Zhao, E. Wang, and C. Yin, "An experimental investigation of the effects of femtosecond laser helical drilling: influence of process parameters," *IOP Conference Series: Materials Science and Engineering*, vol. 265, Article ID 012014, 2017.

[18] H. Zhang, J. Di, M. Zhou, Y. Yan, and R. Wang, "An investigation on the hole quality during picosecond laser helical drilling of stainless steel 304," *Applied Physics A*, vol. 119, no. 2, pp. 745–752, 2015.

[19] H. Zhang, M. Zhou, Y. Wang, X. Zhang, Y. Yan, and R. Wang, "Development of a quantitative method for the characterization of hole quality during laser trepan drilling of high-temperature alloy," *Applied Physics A*, vol. 122, no. 2, p. 74, 2016.

[20] X. Zhu, A. Y. Naumov, D. M. Villeneuve, and P. B. Corkum, "Influence of laser parameters and material properties on micro drilling with femtosecond laser pulses," *Applied Physics A*, vol. 69, no. 1, pp. S367–S371, 1999.

[21] C. Fornaroli, J. Holtkamp, and A. Gillner, "Laser-beam helical drilling of high quality micro holes," *Physics Procedia*, vol. 41, pp. 661–669, 2013.

[22] T. L. See, Z. Liu, H. Liu et al., "Effect of geometry measurements on characteristics of femtosecond laser ablation of HR4 nickel alloy," *Optics and Lasers in Engineering*, vol. 64, pp. 71–78, 2015.

[23] S. Mishra and V. Yadava, "Modeling and optimization of laser beam percussion drilling of thin aluminum sheet," *Optics & Laser Technology*, vol. 48, pp. 461–474, 2013.

[24] C. Foehl, D. Breitling, K. Jasper, J. Radtke, and F. Dausinger, "Precision drilling of metals and ceramics with short-and ultrashort-pulsed solid state lasers," *2nd International Symposium on Laser Precision Microfabrication*, vol. 4426, pp. 104–107, 2002.

[25] C. P. Yin, Z. P. Wu, Y. W. Dong, Y. C. You, and T. Liao, "Femtosecond laser helical drilling of nickel-base single-crystal super-alloy: effect of machining parameters on geometrical characteristics of micro-holes," *Advances in Production Engineering and Management*, vol. 14, no. 4, 2019.

[26] S. I. Anisimov, B. L. Kapeliovich, and T. L. Perelman, "Electron emission from metal surfaces exposed to ultrashort laser pulses," *Zhurnal Eksperimental'noi i Teoreticheskoi Fiziki*, vol. 66, no. 2, pp. 375–377, 1974.

[27] A. Pineau, B. Chimier, S. X. Hu, and G. Duchateau, "Improved modeling of the solid-to-plasma transition of polystyrene ablator for laser direct-drive inertial confinement fusion hydrocodes," *Physical Review*, vol. 104, no. 1-2, Article ID 015210, 2021.

[28] G. Duchateau, S. X. Hu, A. Pineau et al., "Modeling the solid-to-plasma transition for laser imprinting in direct-drive inertial confinement fusion," *Physical Review*, vol. 100, no. 3, Article ID 033201, 2019.

[29] V. V. Zhakhovskii, N. A. Inogamov, Y. V. Petrov, S. I. Ashitkov, and K. Nishihara, "Molecular dynamics simulation of femtosecond ablation and spallation with different interatomic potentials," *Applied Surface Science*, vol. 255, no. 24, pp. 9592–9596, 2009.

[30] C. Momma, S. Nolte, B. Alvensleben, F. V. Alvensleben, and A. Tünnermann, "Precise laser ablation with ultrashort pulses," *Applied Surface Science*, vol. 109-110, pp. 15–19, 1997.

[31] C. Wu and L. V. Zhigilei, "Microscopic mechanisms of laser spallation and ablation of metal targets from large-scale molecular dynamics simulations," *Applied Physics A*, vol. 114, no. 1, pp. 11–32, 2014.